

**Gain-assisted high-dimensional self-trapped laser beams at very low light levels**Hui-jun Li,<sup>1</sup> Liangwei Dong,<sup>2</sup> Chao Hang,<sup>3</sup> and Guoxiang Huang<sup>1,3,\*</sup><sup>1</sup>*Institute of Nonlinear Physics, Zhejiang Normal University, Jinhua 321004, Zhejiang, China*<sup>2</sup>*Department of Physics, Zhejiang Normal University, Jinhua 321004, Zhejiang, China*<sup>3</sup>*State Key Laboratory of Precision Spectroscopy, East China Normal University, Shanghai 200062, China*

(Received 27 July 2010; published 23 February 2011)

We propose a scheme to generate high-dimensional self-trapped laser beams at a very low light intensity via atomic coherence. The system we consider is a resonant four-level atomic ensemble, working in an active Raman gain regime and at room temperature. We derive a high-dimensional nonlinear envelope equation for a signal field with a specific saturable nonlinearity. We show that because of the quantum interference effect induced by a control field, the imaginary part of the coefficients of the signal-field envelope equation can be much smaller than their real part. We demonstrate that the system supports gain-assisted, stable, high-dimensional spatial optical solitons and long-lifetime vortices, which can be produced with light power at the microwatt level.

DOI: [10.1103/PhysRevA.83.023816](https://doi.org/10.1103/PhysRevA.83.023816)

PACS number(s): 42.65.Tg, 05.45.Yv

**I. INTRODUCTION**

Spatial optical solitons are special types of optical wave packets appearing as a result of interplay between diffraction and nonlinearity. Their study is of special interest because of their rich nonlinear physics and important practical applications [1–5]. Up to now, most spatial optical solitons are produced in passive optical media, in which far-off resonance excitation schemes are employed in order to avoid significant optical absorption. As a result, a very high light intensity is usually needed to obtain enough nonlinearity for balancing the diffraction effect.

In recent years, much interest has focused on the wave propagation in highly resonant optical media via electromagnetically induced transparency (EIT). EIT can be used not only for suppressing optical absorption but also for acquiring ultraslow group velocity, for enhancing Kerr nonlinearity [6], and for temporal [7–9] and spatial [10–13] optical solitons and vortices in resonant nonlinear systems. However, the EIT-based schemes have some inherent drawbacks such as the probe attenuation and spreading at room temperature and the long response time because of the character of ultraslow propagation.

Parallel to the study of EIT, much attention has also been paid to the wave propagation in resonant optical media with active Raman gain (ARG) [14–23]. Contrary to the EIT-based scheme, which is absorptive in nature, the central idea of the ARG scheme is that the signal field operates in stimulated Raman emission mode, and hence attenuation of the signal field can be completely eliminated and a superluminal propagation of the signal field can be realized [14–23]. In addition, it has been shown recently by Deng and Payne [24] that a gain-assisted giant Kerr effect can also be obtained by using ARG media. Based on these results, gain-assisted temporal optical solitons of superluminal propagating velocity have been predicted [25–27]. However, there has been no report on the study of gain-assisted spatial optical solitons and vortices in the ARG-based systems.

In this article, we propose a scheme to generate high-D spatial optical solitons and vortices in a four-level ARG system. We derive a high-D nonlinear Schrödinger (NLS) equation for the signal-field envelope and show that, by means of the quantum interference effect induced by a control field, the imaginary part of the coefficients of the envelope equation can be much smaller than their real part. The high-D NLS equation obtained has an interesting type of saturable nonlinearity, which allows solutions of gain-assisted high-D spatial optical solitons and vortices. Owing to the resonant character of the system, the high-D self-trapped nonlinear laser beams obtained can be produced by using very low light power.

The article is arranged as follows. Section II gives a simple introduction of the theoretical model and derives the high-D NLS equation. Section III investigates the formation and propagation of high-D spatial optical solitons and vortices and discusses their interaction and stability. The last section summarizes the main results of our work.

**II. MODEL AND ENVELOPE EQUATION**

The model under consideration is shown in Fig. 1. A weak signal field (with center angular frequency  $\omega_S$ ), a strong pump field (with center angular frequency  $\omega_P$ ), and a strong control field (with center angular frequency  $\omega_C$ ) interact resonantly with a  $N$ -type four-level system. The electric-field vector in the system is given by  $\mathbf{E} = \sum_{l=P,S,C} \mathbf{e}_l \mathcal{E}_l \exp[i(\mathbf{k}_l \cdot \mathbf{r} - \omega_l t)] + \text{c.c.}$ , where  $\mathbf{e}_l$  ( $\mathbf{k}_l$ ) is the polarization direction (wave vector) of  $l$ th field with envelope  $\mathcal{E}_l$ . The Hamiltonian of the system in the interaction picture reads  $\hat{H}_{\text{int}} = -\hbar \sum_{j=1}^4 \Delta_j |j\rangle \langle j| - \hbar(\Omega_P |3\rangle \langle 1| + \Omega_S |3\rangle \langle 2| + \Omega_C |4\rangle \langle 2| + \text{H.c.})$ . Here  $\Delta_3 = \omega_P - (\omega_3 - \omega_1)$ ,  $\Delta_2 = \omega_P - \omega_S - (\omega_2 - \omega_1)$  and  $\Delta_4 = \omega_P - \omega_S + \omega_C - (\omega_4 - \omega_1)$  are, respectively, the one-, two-, and three-photon detunings;  $\Omega_P \equiv (\mathbf{e}_P \cdot \mathbf{p}_{13}) \mathcal{E}_P / \hbar$ ,  $\Omega_S \equiv (\mathbf{e}_S \cdot \mathbf{p}_{23}) \mathcal{E}_S / \hbar$ , and  $\Omega_C \equiv (\mathbf{e}_C \cdot \mathbf{p}_{24}) \mathcal{E}_C / \hbar$  are, respectively, the half Rabi frequency of the pump, signal, and control fields, with  $\mathbf{p}_{ij}$  being the electric dipole matrix element associated with the transition from state  $|i\rangle$  to state  $|j\rangle$ .

Using the Schrödinger equation  $i\hbar \partial |\Psi(t)\rangle_{\text{int}} / \partial t = \hat{H}_{\text{int}} |\Psi(t)\rangle_{\text{int}}$  with  $|\Psi(t)\rangle_{\text{int}} = (A_1, A_2, A_3, A_4)^T$  and under

\*gxhuang@zjnu.edu.cn

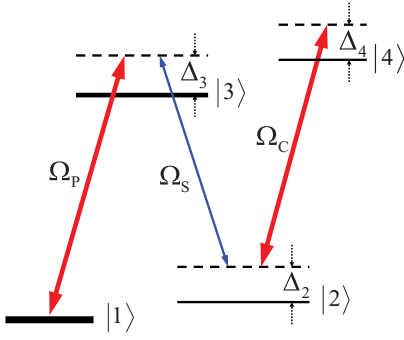


FIG. 1. (Color online) Excitation scheme of lifetime-broadened four-state atomic system interacting with a strong pump field (with half Rabi frequency  $\Omega_P$ ), a strong control field (with half Rabi frequency  $\Omega_C$ ), and a weak signal field (with half Rabi frequency  $\Omega_S$ );  $|j\rangle$  ( $j = 1, 2, 3, 4$ ) are bare atomic states;  $\Delta_3$ ,  $\Delta_2$ , and  $\Delta_4$  are one-photon, two-photon, and three-photon detunings, respectively.

electric dipole and rotating-wave approximations, we obtain the equation of motion for  $A_j$ :

$$\left(i \frac{\partial}{\partial t} + d_2\right) A_2 + \Omega_S^* A_3 + \Omega_C^* A_4 = 0, \quad (1a)$$

$$\left(i \frac{\partial}{\partial t} + d_3\right) A_3 + \Omega_P A_1 + \Omega_S A_2 = 0, \quad (1b)$$

$$\left(i \frac{\partial}{\partial t} + d_4\right) A_4 + \Omega_C A_2 = 0, \quad (1c)$$

with  $\sum_{j=1}^4 |A_j|^2 = 1$  and  $d_j = \Delta_j + i\gamma_j$  ( $j = 2, 3$ );  $\gamma_j$  is the decay rate of the state  $|j\rangle$ .

Under slowly varying envelope approximation, the Maxwell equation for the signal field is reduced to

$$i \left( \frac{\partial}{\partial z} + \frac{1}{c} \frac{\partial}{\partial t} \right) \Omega_S + \frac{c}{2\omega_S} \nabla_{\perp}^2 \Omega_S + \kappa A_3 A_2^* = 0, \quad (2)$$

where  $\nabla_{\perp}^2 = \partial^2/\partial x^2 + \partial^2/\partial y^2$ ,  $\kappa = N\omega_S |\mathbf{e}_S \cdot \mathbf{p}_{23}|^2 / (2\epsilon_0 \hbar c)$ , with  $N$  being atomic concentration. For simplicity, the signal field has been assumed to propagate in the  $z$  direction, that is,  $\mathbf{k}_S = \mathbf{e}_z k_S$ .

We assume that atoms are initially populated in the state  $|1\rangle$ . Since the system works at room temperature, the Doppler effect resulting from thermal motion of atoms is significant. In order to suppress the large gain of the signal field and the Doppler effect, we assume that one-photon detuning  $\Delta_3$  is large enough. The steady state solution of Eqs. (1) and (2) is given by  $A_1^{(0)} = 1/\sqrt{1 + |\Omega_P/d_3|^2}$ ,  $A_2^{(0)} = 0$ ,  $A_3^{(0)} = -\Omega_P/(d_3\sqrt{1 + |\Omega_P/d_3|^2})$ ,  $A_4^{(0)} = 0$ . By assuming  $A_j - A_j^{(0)}$  and  $\Omega_S$  proportional to  $\exp[i(Kz - \omega t)]$ , it is easy to get the linear dispersion relation of the signal field:

$$K(\omega) = \frac{\omega}{c} - \frac{\kappa |A_3^{(0)}|^2 (\omega - d_4^*)}{|\Omega_C|^2 - (\omega - d_2^*)(\omega - d_4^*)}, \quad (3)$$

where  $\omega$  and  $K$  are deviation of frequency and wave vector of the signal field, respectively. Figure 2 shows the real part  $\text{Re}K(\omega)$  (solid line) and the negative imaginary part  $-\text{Im}K(\omega)$  (dashed line) of  $K$  as a function of  $\omega$  with realistic system parameters for  $^{87}\text{Rb}$  atoms [24]. We see that  $-\text{Im}K(\omega)$

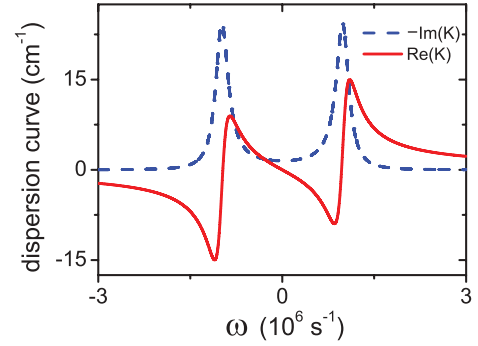


FIG. 2. (Color online) Real part  $\text{Re}K(\omega)$  (solid line) and negative imaginary part  $-\text{Im}K(\omega)$  (dashed line) of the linear dispersion relation of the signal field as functions of  $\omega$ .

displays a structure of a gain spectrum hole, where signal-field gain is largely suppressed. The width of the gain spectrum hole is proportional to the intensity of the control field. The physical reason for the appearance of such a gain spectrum hole is the quantum interference effect induced by the control field [27,28].

We focus on the steady state regime of the system, in which time-derivative terms in Eqs. (1) and (2) can be neglected. Such a regime can be realized under the condition  $|d_j|\tau_0 \gg 1$ , where  $\tau_0$  is the pulse length of the signal field. In this case, using Eq. (1), we obtain  $A_1 = DA_3/(\Omega_P D_1)$ ,  $A_2 = d_4 \Omega_S^* A_3 / D_1$ ,  $A_4 = -\Omega_C \Omega_S^* A_3 / D_1$ , with  $|A_3|^2 = [1 + |d_4 \Omega_S / D_1|^2 + |D/(\Omega_P D_1)|^2 + |\Omega_C \Omega_S / D_1|^2]^{-1}$ ,  $D_1 = |\Omega_C|^2 - d_2 d_4$ , and  $D = -d_3 D_1 - d_4 |\Omega_S|^2$ . Then Eq. (2) reduces to the (2+1)-D NLS equation with saturable nonlinearity:

$$i \frac{\partial \Omega_S}{\partial z} + \frac{c}{2\omega_S} \nabla_{\perp}^2 \Omega_S + \frac{\kappa d_4^* D_1}{G} \frac{\Omega_S}{1 + \alpha |\Omega_S|^2 + \beta |\Omega_S|^4} = 0, \quad (4)$$

with  $\alpha = [ |d_4|^2 + |\Omega_C|^2 + 2|d_4/\Omega_P|^2 \text{Re}(d_3 D_1/d_4) ] / G$ ,  $\beta = |d_4/\Omega_P|^2 / G$ , and  $G = |D_1|^2 (1 + |d_3/\Omega_P|^2)$ .

In linear approximation, the signal beam spreads during propagation because of the diffraction of the system. In order to arrest such spreading and obtain a stable signal-beam propagation, a natural way is to use the saturable nonlinear effect of the system. To explore such a possibility, we write Eq. (4) into the dimensionless form

$$i \frac{\partial u}{\partial s} + \left( \frac{\partial^2}{\partial \xi^2} + \frac{\partial^2}{\partial \eta^2} \right) u + \text{Re}(\delta) \frac{u}{1 + \sigma |u|^2 + \zeta |u|^4} = P[u], \quad (5)$$

where  $s = z/L_D$ ,  $(\xi, \eta) = (x, y)/R_{\perp}$ , and  $u = \Omega_S/U_0$ , with  $L_D (\equiv 2R_{\perp}^2 \omega_S/c)$ ,  $R_{\perp}$ , and  $U_0$  being, respectively, characteristic diffraction length, beam radius, and half Rabi frequency of the signal field. The function on the right-hand side (rhs) of Eq. (5) is defined by  $P[u] = -i \text{Im}(\delta) u / [1 + \sigma |u|^2 + \zeta |u|^4]$ . The coefficients in Eq. (5) are given by  $\sigma = U_0^2 \alpha$ ,  $\zeta = \beta U_0^4$ , and  $\delta = \text{Re}(\delta) + i \text{Im}(\delta)$ , with  $\text{Re}(\delta) = \Delta_4 \kappa D_1 L_D / G$  and  $\text{Im}(\delta) = -\gamma_4 \kappa \gamma_4 D_1 L_D / G$ . Notice that  $\sigma$  and  $\zeta$  are real, but  $\delta$  is complex. Notice that since  $\text{Im}(\delta) < 0$ , the term  $P[u]$  in Eq. (5) is not an absorption but a gain one.

Now we make an estimation of realistic values of the coefficients appeared in Eq. (5). We consider a typical warm atomic vapor of  $^{87}\text{Rb}$  used in Ref. [24]. System parameters are given by  $\gamma_2 = 150\text{ Hz}$ ,  $\gamma_3 = 250\text{ MHz}$ ,  $\gamma_4 = 250\text{ kHz}$ ,  $\kappa = 7.04 \times 10^9\text{ cm}^{-1}\text{s}^{-1}$ , and  $\omega_S = 2.37 \times 10^{15}\text{ s}^{-1}$ . Other parameters are chosen as  $\Delta_2 = 0$ ,  $\Delta_3 = -2.0 \times 10^9\text{ s}^{-1}$ ,  $\Delta_4 = -3.0 \times 10^8\text{ s}^{-1}$ ,  $\Omega_P = 8.0 \times 10^7\text{ s}^{-1}$ ,  $\Omega_C = 6.0 \times 10^7\text{ s}^{-1}$ , and  $R_{\perp} = 4.0 \times 10^{-3}\text{ cm}$ . With these parameters, we obtain  $L_D = 2.53\text{ cm}$ ,  $U_0 = 1.04 \times 10^8\text{ s}^{-1}$ ,  $\sigma = 1.0$ ,  $\zeta = 0.19$ , and  $\delta = -11.66 - 0.01i$ . Because  $\text{Im}(\delta) \ll \text{Re}(\delta)$ , the term  $P[u]$  on the rhs of Eq. (5) can be taken as a perturbation. Consequently, in leading-order approximation, Eq. (5) becomes a NLS equation without gain. Such a result is interesting because in usual undriven resonant systems, one obtains envelope equations with very strong gain or dissipation, that is, the coefficients of the envelope equations have imaginary parts that are of the same order of corresponding real parts. The physical reason for so small an imaginary part in the coefficients of the envelope equation [Eq. (5)] is the quantum interference effect induced by the control field.

NLS equations with saturable nonlinearity have been studied for many years [29–31]. In many cases investigated so far, the term related to saturable nonlinearity is of the form  $f(I)u$ , with  $I = |u|^2$ . Usually, in nonresonant systems,  $f(I)$  takes the form  $n_0/(1 + I/I_0)$ , or  $n_2 I/(1 + I/I_0)$ , with  $n_0$ ,  $n_2$ , and  $I_0$  being constants [2,3,5,32]. In resonant EIT systems,  $f(I)$  takes the form  $n_0/(1 + I/I_0)$  (three level) [12] or a very complicated form (four level) [10]. However, the saturable nonlinearity we obtained in the present four-level ARG system is very specific and has the form  $f(I) = n_0/(1 + I/I_0 + I^2/I_1^2)$ , with  $n_0$ ,  $I_0$  and  $I_1$  being constants.

### III. HIGH-DIMENSIONAL SPATIAL OPTICAL SOLITONS AND VORTICES

We now investigate the possibility of spatial optical solitons and vortices supported by saturable nonlinearity, based on the NLS equation [Eq. (5)]. Our strategy is as follows. We first get soliton or vortex solutions in the leading-order approximation (i.e., the perturbation  $P[u]$  is set to zero). Then we solve Eq. (5) by taking the leading-order solutions as initial conditions to obtain the soliton or vortex solutions of Eq. (5) numerically. In fact, the solutions in the leading-order approximation are already quite accurate because  $\text{Im}(\delta)/\text{Re}(\delta) \approx 10^{-3}$ .

In the leading-order approximation, the solution of Eq. (5) has the form  $u = \Psi(r) \exp[i(\mu + \text{Re}(\delta))s + im\phi]$ ; here  $r^2 = \xi^2 + \eta^2$ ,  $\mu$  is the propagation constant, and  $m(\geq 0)$  is the winding number. The solution for  $m = 0$  corresponds to a soliton, while for  $m \neq 0$ , the solution corresponds to a vortex with topological charge  $m$ . Boundary conditions are  $\partial\Psi/\partial r = 0$  at  $r = 0$  and  $\Psi = 0$  at  $r \rightarrow \infty$  for  $m = 0$  (for solitons) or  $\Psi = 0$  at  $r = 0$  and  $r \rightarrow \infty$  for  $m > 0$  (for vortices).

#### A. Solitons

The soliton solution corresponds to the winding number  $m = 0$ . We solve Eq. (5) by using a Newton iteration method [33], with  $\mu = 2.0$ ,  $\delta = -11.6 - 0.01i$ ,  $\sigma = 1.0$ , and  $\zeta = 0.19$ . Figure 3 shows the result of our numerical simulation. Figures 3(a)–3(c) are soliton profiles for  $s = 0$ ,  $s = 5$ , and

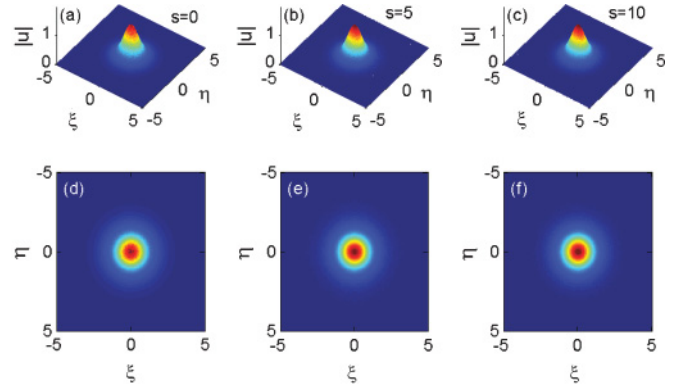


FIG. 3. (Color online) Soliton profile  $|u|$  as a function of coordinates  $\xi$ ,  $\eta$ , and  $s$ , obtained by numerically solving Eq. (5). (a) Initial profile of the soliton ( $s = 0$ ). (b, c) Soliton profiles when propagating to 5 ( $s = 5$ ) and 10 ( $s = 10$ ) diffraction lengths, respectively. (d–f) 2-D projection plots corresponding to (a), (b), and (c), respectively.

$s = 10$  (in units of  $L_D = 2.53\text{ cm}$ ), respectively. Figures 3(d)–3(f) are 2-D projection plots corresponding to Figures 3(a)–3(c), respectively. For checking the stability of the soliton, in the simulation, we have added a small randomness  $\rho_{\text{ran}}$  to the initial condition, that is,  $u = u_{\text{sol}}(1 + \rho_{\text{ran}})$ , with  $|\rho_{\text{ran}}| = 0.1$ . From Fig. 3, we see the soliton keeps its shape after propagating to 10 diffraction length (i.e.,  $s = 10$ ). Hence Eq. (5) indeed admits a soliton solution, and this solution is fairly stable during propagation.

We have also investigated collisions between two solitons by using an accelerated imaginary-time evolution method [34]. Shown in Fig. 4 are profiles of amplitude  $|u|$  as a function of  $\xi$ ,  $\eta$ , and  $s$  for two-soliton collisions. The physical parameters are chosen to be the same as in Fig. 3. The lower part of the figure corresponds to projecting (to the  $\xi$ - $\eta$  plane) plots of the upper part. Note that in the upper part of the figure, 3-D plots have been projected into the  $\eta = 0$  plane. From the figure, we see that soliton collisions display an elastic character; two solitons are attractive for  $\Delta\phi = 0$  but repulsive for  $\Delta\phi = \pi$ .

It is easy to get the peak generation power of the spatial optical soliton obtained previously, which is given by  $\bar{P}_{\text{max}} = 2\epsilon_0 c n_S S_0 (\hbar/|\mathbf{p}_{23}|)^2 U_0^2 |u_{\text{max}}|^2$ , with  $n_S$  and  $S_0$  being the reflective index and the cross-sectional area of the signal beam, respectively. Taking  $S_0 = \pi R_{\perp}^2 \approx 0.5 \times 10^{-4}\text{ cm}^2$ ,  $|\mathbf{p}_{23}| = 2.1 \times 10^{-27}\text{ cm C}$ , and using the other parameters given earlier, we obtain  $\bar{P}_{\text{max}} = 2.32\text{ }\mu\text{W}$ . Hence the spatial optical soliton in the present system can be generated at very low light power, which is much different from the optical soliton generation schemes using passive media, where much higher generation power is required.

#### B. Vortices

It is well known that vortices of high-D NLS equations are generally unstable. However, saturable nonlinearity may be used to effectively suppress such instability [29–32,35]. For a nonresonant passive system, saturation intensity is very large, and saturation parameters of the system are fixed. However, our present system is a resonant active one, so the situation is thus quite different. On one hand, owing to the resonant character of the system, the saturation intensity is

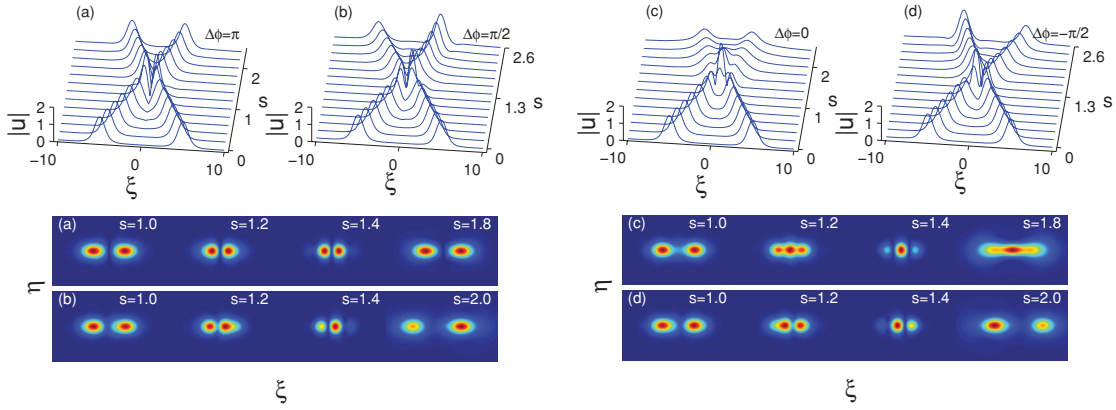


FIG. 4. (Color online) Profiles of amplitude  $|u|$  for two-soliton collisions as a function of  $\xi$  and  $s$  (projection to  $\eta = 0$  plane has been taken). (a–d) Collisions of two solitons with initial relative phases  $\Delta\phi = \pi, \pi/2, 0,$  and  $-\pi/2$ , respectively. (bottom) Corresponding projection (to  $\xi$ - $\eta$  plane) plots of (a–d).

very small. This can be seen as follows. From Eq. (5), the saturable nonlinearity can be obtained by setting  $\sigma |u_{\text{sat}}|^2 \approx 1$ , which gives the saturable electric field of the signal beam as  $|E_{\text{sat}}| = \hbar U_0 / |\mathbf{p}_{23}|$ . Using the numerical values of the physical parameter given earlier, we obtain  $|E_{\text{sat}}| \approx 5$  V/m. On the other hand, the active character of the present system provides us with many adjustable parameters, which can be manipulated to reduce the saturation intensity and increase vortex lifetime. In the following, we shall discuss only how to increase the vortex lifetime by adjusting the half control-field Rabi frequency  $\Omega_C$ . From Eq. (5), we know that the coefficients  $\delta$ ,  $\sigma$ , and  $\zeta$  depend on  $\Omega_C$ , and hence the solution parameters of vortices, that is, the propagation constant  $\mu$  and  $\Psi_{\text{max}}$  (the maximum value of  $\Psi$ ), depend also on  $\Omega_C$ .

Shown in Fig. 5(a) is the relation between  $\Psi_{\text{max}}$  and  $\mu$ , with  $\Omega_C = 6.0 \times 10^7$  s $^{-1}$ . The vortex corresponding to the point  $(\mu, \Psi_{\text{max}}) = (8.56, 3.152)$  in the curve is more stable than the vortex corresponding to the point  $(\mu, \Psi_{\text{max}}) = (5, 1.577)$ . Shown in Fig. 5(b) are curves of saturation parameters  $\sigma$  (solid line) and  $\zeta$  (dashed line) as functions of  $\Omega_C$  for fixed param-

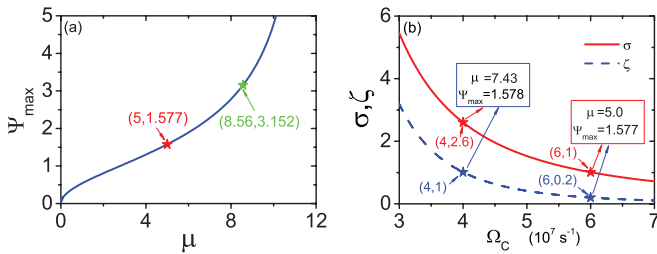


FIG. 5. (Color online) (a)  $\Psi_{\text{max}}$  as a function of propagation constant  $\mu$ , with  $\Omega_C = 6.0 \times 10^7$  s $^{-1}$ . The vortex corresponding to the point  $(\mu, \Psi_{\text{max}}) = (8.56, 3.152)$  in the curve has a longer lifetime than the vortex corresponding to the point  $(\mu, \Psi_{\text{max}}) = (5, 1.577)$ . (b) Curves of saturation parameters  $\sigma$  (solid line) and  $\zeta$  (dashed line) as functions of  $\Omega_C$ . The point  $(4.0, 2.6)$  in the  $\sigma$  curve and the point  $(4, 1)$  in the  $\zeta$  curve correspond to  $(\mu, \Psi_{\text{max}}) = (7.43, 1.578)$ . The point  $(6.0, 1.0)$  in the  $\sigma$  curve and the point  $(6.0, 0.2)$  in the  $\zeta$  curve correspond to  $(\mu, \Psi_{\text{max}}) = (5.0, 1.577)$ . The vortex corresponding to  $(\mu, \Psi_{\text{max}}) = (7.43, 1.578)$  has a longer lifetime than the vortex corresponding to  $(\mu, \Psi_{\text{max}}) = (5.0, 1.577)$ .

eters  $\Delta_2 = 0$ ,  $\Delta_3 = -2.0 \times 10^9$  s $^{-1}$ ,  $\Delta_4 = -3.0 \times 10^8$  s $^{-1}$ , and  $\Omega_P = 8.0 \times 10^7$  s $^{-1}$ . Since the saturation intensity of the signal field is inversely proportional to  $\sigma$  and  $\zeta$ , from the figure, we see that one can reduce the saturation intensity by decreasing  $\Omega_C$ . In the figure, by choosing  $10^7$  s $^{-1}$  as the unit of  $\Omega_C$ , we have illustrated the point  $(\Omega_C, \sigma) = (4.0, 2.6)$  in the  $\sigma$  curve and the point  $(\Omega_C, \zeta) = (4.0, 1.0)$  in the  $\zeta$  curve. Using the values of  $\Omega_C$ ,  $\sigma$ , and  $\zeta$  at these points, we obtain  $(\mu, \Psi_{\text{max}}) = (7.43, 1.578)$ , which has been indicated in the inset in the figure; we have also illustrated the point  $(\Omega_C, \sigma) = (6.0, 1.0)$  in the  $\sigma$  curve and the point  $(\Omega_C, \zeta) = (6.0, 0.2)$  in the  $\zeta$  curve, which correspond to  $(\mu, \Psi_{\text{max}}) = (5.0, 1.577)$ , also indicated in an inset. The vortex corresponding to  $(\mu, \Psi_{\text{max}}) = (7.43, 1.578)$  has a longer lifetime compared with the vortex corresponding to  $(\mu, \Psi_{\text{max}}) = (5.0, 1.577)$ . All these predications have been verified by numerical simulations.

In Fig. 6, we have shown the evolution of  $|u|$  for  $m = 1$  vortex with different distances  $s$ . Figure 6(a) corresponds to the point  $(\mu, \Psi_{\text{max}}) = (5, 1.577)$  of Fig. 5(a), without adding any random perturbation to the initial condition. No deformation of the vortex is found after propagating to  $s = 10$ . However, when a random perturbation  $\rho_{\text{ran}}$  (with  $|\rho_{\text{ran}}| = 0.158$ ) is added into the initial condition, that is,  $u = u_{\text{vor}}(1 + \rho_{\text{ran}})$ , the vortex is stable until propagating to  $s = 2.4$ , but it deforms after  $s = 2.4$  and disintegrates into two solitons, as shown clearly in Fig. 6(b). Plotted in Fig. 6(c) is the result of the evolution of a large-amplitude  $m = 1$  vortex corresponding to the point  $(8.56, 3.152)$  of Fig. 5(a). In this case, the vortex has a longer lifetime in comparison with the case shown in Fig. 6(b) because the vortex can propagate to a longer distance even when a random perturbation is added to the initial condition. Of course, it splits into two solitons at a large distance.

All evolution figures in Fig. 6(a)–Fig. 6(c) are obtained for  $\Omega_C = 6.0 \times 10^7$  s. In order to demonstrate the effect of different saturation parameters, in Fig. 6(d), we have shown the evolution of  $m = 1$  vortex for  $\Omega_C = 4.0 \times 10^7$  s, which corresponds to  $(\mu, \Psi_{\text{max}}) = (7.43, 1.578)$  of Fig. 5(b). We see that in this case, the vortex is also relatively stable compared with that shown in Fig. 6(b).

Shown in Fig. 7 are the evolution plots of the  $m = 2$  vortex for four different propagating distances  $s$ . Figure 7(a)

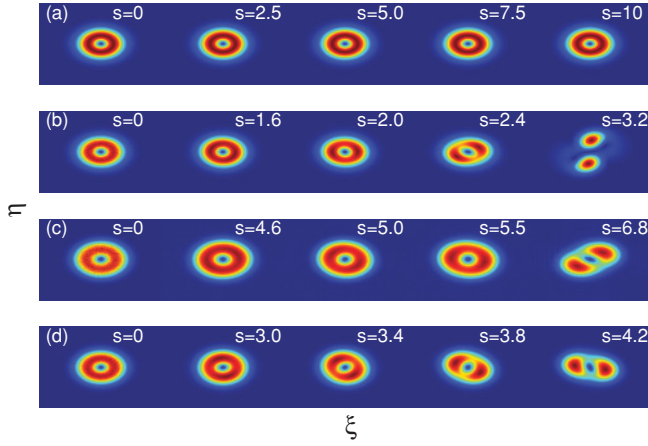


FIG. 6. (Color online) Evolution of amplitude  $|u|$  of  $m = 1$  vortex as a function of  $(\xi, \eta)$ , with different propagating distances  $s$ . (a) Evolution corresponding to the point  $(\mu, \Psi_{\max}) = (5, 1.577)$  of Fig. 5(a) without adding any random perturbation. (b) Evolution when a random perturbation is added into the initial condition. The vortex keeps its shape until propagating to  $s = 2.4$ , but it deforms after  $s = 2.4$  and then disintegrates into two solitons. (c) Evolution of a large-amplitude vortex corresponding to the point  $(\mu, \Psi_{\max}) = (8.56, 3.152)$  of Fig. 5(a). The vortex has a longer lifetime compared with the case shown in (b), but it splits into two solitons at large  $s$ . (d) Evolution corresponding to  $\Omega_C = 4.0 \times 10^7$  s, which corresponds to  $(\mu, \Psi_{\max}) = (7.43, 1.578)$  of Fig. 5(b).

is the vortex evolution for  $(\mu, \Psi_{\max}) = (5, 1.565)$ , without adding any random perturbation to the initial condition. We see that, different from the  $m = 1$  vortex, the  $m = 2$  vortex cannot keep its shape even with no random perturbation added into the initial condition. At  $s = 6.25$ , the vortex splits into four solitons. When a random perturbation  $\rho_{\text{ran}}$  (with

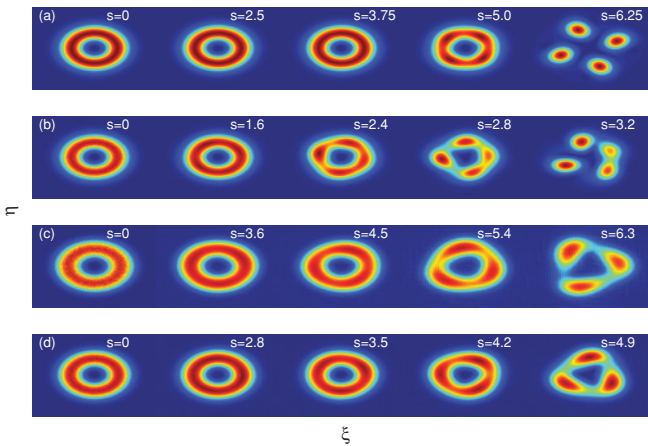


FIG. 7. (Color online) Evolution plots of the  $m = 2$  vortex as functions of  $(\xi, \eta)$ , with different propagating distances  $s$ . (a) Vortex evolution based on Eq. (5) for  $(\mu, \Psi_{\max}) = (5, 1.565)$  without adding any random perturbation to the initial condition. (b) Vortex evolution when a random perturbation is added into the initial condition. (c) Evolution of a large-amplitude  $m = 2$  vortex corresponding to  $(\mu, \Psi_{\max}) = (8.56, 3.152)$ . (d) Evolution of  $m = 2$  vortex corresponding to  $\Omega_C = 4.0 \times 10^7$  s, which corresponds to  $(\mu, \Psi_{\max}) = (7.43, 1.566)$ .

$|\rho_{\text{ran}}| = 0.157$ ) is added to the initial condition, the vortex displays instability in earlier stages ( $s = 2.4$ ). At  $s = 2.8$ , it splits into four solitons, as shown in Fig. 7(b). Figure 7(c) shows the result of the evolution of a large-amplitude  $m = 2$  vortex corresponding to  $(\mu, \Psi_{\max}) = (8.56, 3.152)$ . We see that the large-amplitude vortex is relatively stable compared with the (small-amplitude) vortex of Fig. 7(b). However, it disintegrates into three (not four) solitons at a long evolution distance.

We have also simulated the evolution of the  $m = 2$  vortex by changing the Rabi frequency of the control field. Shown in Fig. 7(d) is the evolution of the  $m = 2$  vortex for  $\Omega_C = 4.0 \times 10^7$  s, which corresponds to  $(\mu, \Psi_{\max}) = (7.43, 1.566)$ . We see that the vortex in this case is also relatively stable in comparison with that shown in Fig. 7(b). Generally, by manipulating the parameters of the system, we can control the lifetime of the vortex freely. In particular, when the control-field intensity decreases a small amount, the lifetime of the vortex can increase significantly. In addition, it is easy to show that the peak generation powers of the  $m = 1$  and  $m = 2$  vortices are also at a microwatt level.

#### IV. DISCUSSION AND SUMMARY

Generally, the vortices found in the system are unstable, mainly because of symmetry-breaking azimuthal perturbations. However, as shown, the instability can be very weak, that is, the vortices can have long lifetimes and hence be observable in experiment and useful in practical applications. Because our system is an active one, we can control the weak instability of the vortices by manipulating the system parameters at will. In addition, there exists a parameter domain in which the vortices are stable, which can be illustrated as follows. Notice that Eq. (5), after making the transformation  $u = v \exp(i\delta s)$ , can be reduced to the cubic-quintic NLS equation

$$i \frac{\partial v}{\partial s} + \left( \frac{\partial^2}{\partial \xi^2} + \frac{\partial^2}{\partial \eta^2} \right) v - \delta \sigma |v|^2 v - \delta(\zeta - \sigma^2) |v|^4 v = 0 \quad (6)$$

if  $\sigma |u|^2 + \zeta |u|^4 \ll 1$ , which can be realized when (i) the signal field is weak and (ii) the saturation intensity is large, which can be achieved easily by selecting the system parameters. Under the condition

$$\delta \sigma = -1, \quad \delta(\zeta - \sigma^2) = 1, \quad (7)$$

Eq. (6) can be transferred into the standard cubic-quintic NLS equation  $i(\partial v / \partial s) + (\partial^2 / \partial \xi^2 + \partial^2 / \partial \eta^2)v + |v|^2 v - |v|^4 v = 0$ , which admits stable vortices [35]. Condition (7) can be easily fulfilled in our system. For instance, by choosing  $\Delta_3 = -1.0 \times 10^9$  s $^{-1}$ ,  $\Delta_4 = -1.69\Delta_3$ ,  $\Omega_P = \Omega_C = -0.1\Delta_3$ ,  $U_0 = -0.44\Delta_3$ ,  $R_{\perp} = 2.516 \times 10^{-3}$  cm, one obtains  $\sigma \approx -0.09$ ,  $\zeta \approx 0.10$ , and thus condition (7) is well satisfied. In this parameter domain, the vortices are very stable, which has been verified in our numerical simulation.

In conclusion, we have proposed a scheme for generating high-D self-trapped laser beams at a very low light intensity via atomic coherence. The system we have considered is an ensemble of resonant four-level atoms, working in an active Raman gain regime and at room temperature. We have derived

a  $(2 + 1)$ -D NLS equation for the signal-field envelope with a specific saturable nonlinearity. We have shown that because of the quantum interference effect induced by a control laser field, the imaginary part in coefficients of the NLS equation can be much smaller than their real part. We have demonstrated that the system supports stable high-D spatial optical solitons and long-lifetime vortices, which can be produced with light power at the microwatt level. The results presented here may be useful for understanding the nonlinear property of coherent atomic systems and guiding experimental findings of spatial solitons and vortices with very low generation power, which may have

potential applications in optical information processing and engineering.

#### ACKNOWLEDGMENTS

The authors thank Vladimir V. Konotop for useful discussions and Jianke Yang for helpful suggestions on our numerical simulations. This work was supported by the NSF-China under Grant No. 10874043, No. 10947137, and No. 10974181 and by the NSF-Zhejiang province of China under Grant No. Y6100355.

- 
- [1] G. I. Stegeman and M. Segev, *Science* **286**, 1518 (1999).
  - [2] Y. S. Kivshar and G. P. Agrawal, *Optical Solitons: From Fibers to Photonic Crystals* (Academic, New York, 2003).
  - [3] Y.-F. Chen, K. Beckwitt, F. W. Wise, and B. A. Malomed, *Phys. Rev. E* **70**, 046610 (2004).
  - [4] B. A. Malomed, D. Mihalache, F. Wise, and L. Torner, *J. Phys. B* **7**, R53 (2005).
  - [5] M. J. Paz-Alonso and H. Michinel, *Phys. Rev. Lett.* **94**, 093901 (2005).
  - [6] M. Fleischhauer, A. Imamoglu, and J. P. Marangos, *Rev. Mod. Phys.* **77**, 633 (2005).
  - [7] Y. Wu and L. Deng, *Phys. Rev. Lett.* **93**, 143904 (2004).
  - [8] G. Huang, L. Deng, and M. G. Payne, *Phys. Rev. E* **72**, 016617 (2005).
  - [9] C. Hang and G. Huang, *Phys. Rev. A* **77**, 033830 (2008).
  - [10] T. Hong, *Phys. Rev. Lett.* **90**, 183901 (2003).
  - [11] H. Michinel, M. J. Paz-Alonso, and V. M. Perez-Garcia, *Phys. Rev. Lett.* **96**, 023903 (2006).
  - [12] H. Jiang, H. Chen, and S. Zhu, *Phys. Rev. E* **73**, 046601 (2006).
  - [13] A. Alexandrescu, H. Michinel, and V. M. Perez-Garcia, *Phys. Rev. A* **79**, 013833 (2009).
  - [14] R. Y. Chiao and A. M. Steinberg, in *Progress in Optics*, edited by E. Wolf (Elsevier, Amsterdam, 1997), p. 345.
  - [15] L. J. Wang, A. Kuzmich, and A. Dogariu, *Nature (London)* **406**, 277 (2000).
  - [16] M. S. Bigelow, N. N. Lepeshkin, and R. W. Boyd, *Science* **301**, 200 (2003).
  - [17] M. D. Stenner, D. J. Gauthier, and M. A. Neifield, *Nature (London)* **425**, 695 (2003).
  - [18] R. G. Ghulghazaryan and Y. P. Malakyan, *Phys. Rev. A* **67**, 063806 (2003).
  - [19] K. Kim, H. S. Moon, C. Lee, S. K. Kim, and J. B. Kim, *Phys. Rev. A* **68**, 013810 (2003).
  - [20] L.-G. Wang, N.-H. Liu, Q. Lin, and S.-Y. Zhu, *Phys. Rev. E* **68**, 066606 (2003).
  - [21] M. Janowicz and J. Mostowski, *Phys. Rev. E* **73**, 046613 (2006).
  - [22] K. J. Jiang, L. Deng, and M. G. Payne, *Phys. Rev. A* **74**, 041803(R) (2006).
  - [23] J. Zhang, G. Hernandez, and Y. Zhu, *Opt. Lett.* **31**, 2598 (2006).
  - [24] L. Deng and M. G. Payne, *Phys. Rev. Lett.* **98**, 253902 (2007).
  - [25] G. Huang, C. Hang, and L. Deng, *Phys. Rev. A* **77**, 011803(R) (2008).
  - [26] H.-J. Li, C. Hang, G. Huang, and L. Deng, *Phys. Rev. A* **78**, 023822 (2008).
  - [27] C. Hang and G. Huang, *Opt. Express* **18**, 2952 (2010).
  - [28] G. S. Agarwal and S. Dasgupta, *Phys. Rev. A* **70**, 023802 (2004).
  - [29] W. J. Firth and D. V. Skryabin, *Phys. Rev. Lett.* **79**, 2450 (1997).
  - [30] D. V. Skryabin and W. J. Firth, *Phys. Rev. E* **58**, 3916 (1998).
  - [31] A. S. Desyatnikov, Y. S. Kivshar, and L. Torner, in *Progress in Optics*, edited by E. Wolf (Elsevier Science, Amsterdam, 2005), Vol. 47, Chap. 6, p. 1, and references therein.
  - [32] B. A. Malomed, D. Mihalache, F. Wise, and L. Torner, *J. Opt. B* **7**, 53(R) (2005), and references therein.
  - [33] J. Yang, *J. Comput. Phys.* **228**, 7007 (2009).
  - [34] J. Yang and T. I. Lakoba, *Stud. Appl. Math.* **120**, 265 (2008).
  - [35] I. Towers, A. V. Buryak, R. A. Sammut, B. A. Malomed, L.-C. Crasovan, and D. Mihalache, *Phys. Lett. A* **288**, 292 (2001).